Title

More rapid polar ozone depletion through the reaction of HOCl with HCl on polar stratospheric clouds

Permalink

Journal

ISSN

Author

Prather, Michael J

Publication Date

DOI

Copyright Information

Peer reviewed

C_{60} for K_3C_{60}, which corresponds to a bandwidth of ~200 meV. As a crude approximation one can estimate the bandwidth to be twice the Fermi energy, as the conduction bands are half-filled for Rb_3C_{60}. Our value of $E_F \lesssim 100$ meV then corresponds to a bandwidth of $\lesssim 200$ meV. This is reasonably close to the value inferred from the NMR results and from angle-resolved photo-emission data[25], but smaller than the results of refs 23 and 24. A possible resolution of the discrepancy between the narrow bandwidth inferred from low-energy measurements (NMR, infrared and critical field), and the broader bandwidth obtained by angle-integrated photoemission spectroscopy is discussed by Shen et al.[25]

Thus far we have been considering the frequency scale of the infrared reflectivity changes. The amplitude of the enhancement, $R_s/R_n - 1$, is also useful, as it is related to the d.c. resistivity, ρ_{dc}, of Rb_3C_{60}. This is of particular interest in the present case because of the difficulties in using standard d.c. methods (A.F. Hebard, personal communication). At sufficiently low frequency ($\omega \lesssim 2\Delta$ and $\omega < 1/\tau$, where $1/\tau$ is the elastic scattering rate due to impurities) this relationship can be expressed as $\rho_{dc} \approx (\pi R_n^2/2\omega n^2)(R_s/R_n - 1)^2$ where n is the index of refraction of the sapphire, which is about 3.1 in the far-infrared. Because R_n is always close to 1 in the far infrared, the dependence of the right-hand side on R_n is dominated by the second term, $(R_s/R_n - 1)^2$, reflecting the fact that a material with higher resistivity has a lower normal-state reflectivity and thus a larger maximum value for $R_s/R_n - 1$. From this equation and the data in Fig. 1c for $\omega \lesssim 40$ cm^{-1}, we infer a d.c. resistivity of ~0.4 mΩ cm, which corresponds to a scattering rate of ~150–300 cm^{-1}. The large value of the scattering rate (relative to kT) indicates that it is associated with elastic scattering (disorder). Because scattering due to disorder tends to be strongly pair-breaking for non-zero angular momentum pairing, such a large scattering rate suggests that the pair wavefunction in Rb_3C_{60} is likely to have s-wave symmetry, in agreement with the more direct inference of Uemura et al.[27] based on the temperature dependence of the penetration depth.

Because this scattering rate is larger than the relevant infrared measurement frequencies, infrared and d.c. measurements of ρ_{dc} should agree. We find, however, that the infrared value is about an order of magnitude smaller than the estimates obtained from direct d.c. measurements (A. F. Hebard, personal communication). Presumably this difference is due to the length scale at which one is probing, relative to the grain size of the material (~50 nm for our material). The infrared measurements probe at a length scale of roughly v_F/ω, which is about 10 nm for $\omega \approx 40$ cm^{-1}, whereas the relevant length scale for d.c. measurements is the distance between contacts, which is much longer. On this basis one would expect the infrared result to be closer to the intrinsic value than the contact-based measurement. With the infrared value ($\rho_{dc} \approx 0.4$ mΩ cm), a mean free path, l, of ~2 nm is obtained, whereas from the higher d.c.-based estimates of ρ_{dc}, mean free paths of $l \lesssim 0.4$ nm have been inferred. (To get this result one can use $l = 3\pi^2 (\hbar/e^2)\sigma_{dc}/k_F^2$, where σ_{dc} is the d.c. conductivity). This difference is significant for two reasons: (1) the d.c.-based values of l suggested a mean free path less than the separation between C_{60} molecules, in apparent violation of the Ioffe-Regel guideline, whereas the longer infrared-based value does not, and (2) the d.c.-based value was so short as to suggest a substantial difference between ξ and ξ_0, which would significantly affect the derivation of v_F, whereas the longer infrared-based value is consistent with only a modest difference between ξ and ξ_0, as used above.

Although the details cannot be discussed here, the above estimates of resistivity and energy gap can be used to estimate the electromagnetic penetration depth, λ of Rb_3C_{60}. To do this one can use $\lambda = c/(8A)^{1/2}$ with the dirty limit formula $A \approx 2.2(2\Delta)/\rho_{dc}$, which is appropriate because the disorder-related scattering rate is large relative to 2Δ. ('Dirty' means that the elastic scattering rate is significantly larger than the gap, 2Δ, or,

equivalently, that the elastic mean free path is less than the coherence length.) With the above values of 2Δ and ρ_{dc} this equation implies a penetration depth of 500 ± 100 nm, which is larger than the value expected in the clean limit, but in agreement with estimates based on muon spin resonance[27]. □

1. Hebard, A. F. et al. Nature 350, 600–601 (1991).
2. Zhang, Z., Chen, C.-C., Ketty, S. P., Dai, H. & Leifer, C. M. Nature 353, 333–335 (1991).
3. Glover, R. E. & Tinkham, M. Phys. Rev. 108, 243–256 (1957).
4. Richards, P. L. & Tinkham, M. Phys. Rev. 119, 575–590 (1960).
5. Giaever, I., Hart, H. R. & Megerle, K. Phys. Rev. 126, 941 (1962).
6. Schlesinger, Z. et al. Phys. Rev. B40, 6862–6866 (1989).
7. Zasazinski, J. F. et al. Physica C158, 518–524 (1989).
8. Rosseinsky, M. J. et al. Phys. Rev. Lett. 66, 2830–2833 (1991).
9. McCauley, John P. Jr. et al. J. Am chem. Soc. 113, 8537–8542 (1991).
10. Fleming, R. M. et al. Nature (in the press).
11. Stephens, P. W. et al. Phys. Rev. B (submitted).
12. Schlesinger, Z. et al. Phys. Rev. B41, 11237–11259 (1990).
13. Bonn, D. A. et al. Phys. Rev. B35, 8843–8846 (1987).
14. Schlesinger, Z. et al. Phys. Rev. B36, 5275–5278 (1987).
15. Schlesinger, Z. et al. Phys. Rev. B38, 9284–9286 (1988).
16. Bickers, N. E. et al. Phys. Rev. B42, 67–75 (1990).
17. Tanner, D. B. & Sievers, A. J. Phys. Rev. B8, 1978–1980 (1973).
18. Sparn, G. et al. Phys. Rev. B (submitted).
19. Pippard, A. B. Proc. R. Soc. A216, 547 (1953).
20. Tinkham, M. Introduction to Superconductivity (Krieger, Malabar, 1975).
21. Ashcroft, N. W. & Mermin, N. D. Solid State Physics (Holt, Rinehart & Wilson, New York, 1976).
22. Holczer, K. et al. Phys. Rev. Lett. 67, 271–274 (1991).
23. Erwin, S. C. & Pickett, W. E. Science 254, 842–845 (1991).
24. Chen, C. T. et al. Nature 352, 603–605 (1991).
25. Shen, Z.-X. et al. Phys. Rev. B (submitted).
26. Tycko, R. et al. Science 253, 884–888 (1991).
27. Uemura, Y. J. et al. Nature 352, 605–607 (1991).

More rapid polar ozone depletion through the reaction of HOCl with HCl on polar stratospheric clouds

Michael J. Prather
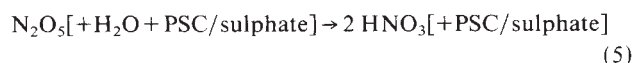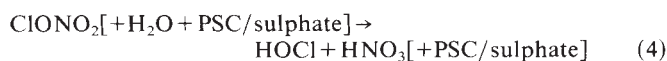
NASA/GISS, 2880 Broadway, New York, New York 10025, USA

THE direct reaction of HOCl with HCl, known to occur in liquid water[1] and on glass surfaces[2], has now been measured on surfaces similar to polar stratospheric clouds[3,4] and is shown here to play a critical part in polar ozone loss. Two keys to understanding the chemistry of the Antarctic ozone hole[5-7] are, one, the recognition that reactions on polar stratospheric clouds transform HCl into more reactive species denoted by ClO_x (refs 8–12) and, two, the discovery of the ClO-dimer (Cl_2O_2) mechanism that rapidly cataly-ses destruction of O_3 (refs 13–15). Observations of high levels of OClO and ClO in the springtime Antarctic stratosphere[16-19] confirm that most of the available chlorine is in the form of ClO_x (refs 20, 21). But current photochemical models[22,23] have difficulty converting HCl to ClO_x rapidly enough in early spring to account fully for the observations[5-7,20,21]. Here I show, using a chemical model, that the direct reaction of HOCl with HCl provides the missing mechanism. As alternative sources of nitrogen-containing oxidants, such as N_2O_5 and $ClONO_2$, have been converted in the late autumn to inactive HNO_3 by known reactions on the sulphate-layer aerosols[24-27], the reaction of HOCl with HCl on polar stratospheric clouds becomes the most important pathway for releasing that stratospheric chlorine which goes into polar night as HCl.

The reaction

$$HCl + HOCl[+PSC] \rightarrow Cl_2[+PSC + H_2O] \qquad (1)$$
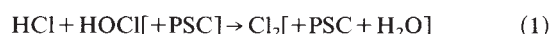
proceeds rapidly[3,4] on both cold water-ice and solid nitric acid trihydrate, but is expected to be slow on sulphuric acid aerosols

unless they are dilute or partially neutralized[3,30]. It probably proceeds through the adsorption of HCl or both species onto the surface, as do the other established heterogeneous reactions that return the adsorbed HCl to the gas phase in a more reactive form[9,10,29-33]. This currently used set of heterogeneous reactions has been measured on both ice (polar stratospheric cloud, PSC, type II) and nitric acid trihydrate (PSC type I).

$$HCl + ClONO_2[+PSC] \rightarrow Cl_2 + HNO_3[+PSC] \qquad (2)$$

$$HCl + N_2O_5[+PSC] \rightarrow ClNO_2 + HNO_3[+PSC] \quad (3)$$

$$ClONO_2[+H_2O + PSC/sulphate] \rightarrow$$
$$HOCl + HNO_3[+PSC/sulphate] \qquad (4)$$

$$N_2O_5[+H_2O + PSC/sulphate] \rightarrow 2\,HNO_3[+PSC/sulphate]$$
$$(5)$$

Experimental data for reactions (2) and (4) suggest[3,4] that the HOCl released from reaction (4) on ice reacts rapidly on the surface with HCl, and thus reaction (2) may be thought of as a two-step process: reaction (4) followed by (1). In either case, the existence of pathway (1) makes the direct effects of PSC chemistry more straightforward: the competition for $ClONO_2$ between reactions (2) and (4) is no longer important, because either path (2) or (4) + (1) results in the conversion of HCl to Cl_2.

The partitioning of chlorine species as the Antarctic goes into polar night is unknown and represents a large uncertainty. Photochemical models indicate that HCl should be the dominant form of chlorine in the wintertime lower stratosphere, but we lack corroborating measurements. Here I first examine how the chlorine partitioning might be set in late autumn as photolytic acitivity ceases, and then focus on the photochemical evolution of ClO_x ($ClO + 2 \times Cl_2O_2 + Cl + 2 \times Cl_2 + OClO$) as the Antarctic vortex comes out of winter in the presence of PSCs (that is, the initial development of the ozone hole from August to October).

Reactions (4) and (5) occur in the laboratory on the surfaces of sulphuric acid/water mixtures[24-27], which are ubiquitous in the lower stratosphere throughout the year. (PSCs are present only during the coldest parts of winter and early spring.) These

reactions have already been incorporated in models of ozone depletion for different concentrations of chlorine and background sulphate aerosols[34-37]. The photochemical evolution of an air parcel at 75° S from equinox (18 March) to late autumn twilight (20 May) is shown in Fig. 1 for cases with and without reactions (4) and (5). With gas-phase chemistry alone, most of the chlorine evolves into HCl with the remainder, ~30%, in $ClONO_2$; negligible amounts of HOCl and ClO_x survive. In this case high concentrations of N_2O_5 and NO_x (which represents $NO + NO_2 + NO_3$) are predicted, in contradiction to most polar observations[38]. If sulphate-layer reactions (4) and (5) are included, they push most of the odd-nitrogen into HNO_3 as expected, and are also important in chlorine chemistry. Compared with gas-phase chemistry, both $ClONO_2$ and HCl are reduced at the end of autumn as HOCl and ClO_x species increase.

By the end of polar night, PSCs (type I or II) are assumed to have completely processed the chlorine and odd-nitrogen species according to reactions (2) and (3) above, leaving 1.2 p.p.b. residual HCl. In addition, the air has become denitrified and dehydrated as observed in the Airborne Antarctic Ozone Experiment[39]. Whereas $ClONO_2$ (0.3 p.p.b.) can oxidize an equivalent amount of HCl, the amount of chlorine in the form ClO_x (0.1 p.p.b.) cannot. The HOCl (0.6 p.p.b.) created during polar night would reduce the residual HCl to 0.6 p.p.b. if we include reaction (1). In either case, gas-phase or sulphate-layer chemistry in the spring, the concentration of HCl carried into winter is higher than that of chlorinated oxidants. Only in the gas-phase case (ruled out here) can the residual N_2O_5 (1.2 p.p.b.) completely convert HCl to ClO_x through reaction (3).

The same photochemical model, now including PSC reactions (1) to (3), continues to follow the evolution of the isolated air parcel at 75° S latitude and 20 km altitude as it comes out of polar night from 29 July (noontime solar zenith angle of 94°) to 14 October (noontime solar zenith angle of 67°). The initial proportions and trends of the principal chlorine species are given in Fig. 1. The air parcel is assumed to be in contact with PSCs throughout the period, and two different chemistries are

FIG. 1 Noon-time mixing ratios of selected species from the photochemical evolution of an isolated air parcel at 75° S, 20 km altitude. The model was initialized on 18 March (volume mixing ratios $O_3 = 2.5 \times 10^{-6}$, $HNO_3 = 5 \times 10^{-9}$, $NO_x = 2 \times 10^{-9}$, $ClONO_2 = 1 \times 10^{-9}$, $HCl = 1.5 \times 10^{-9}$, $BrO = 15 \times 10^{-12}$, $H_2O = 4 \times 10^{-6}$, $H_2 = 0.5 \times 10^{-6}$, $CH_4 = 1 \times 10^{-6}$) and integrated through the autumn, with solar declination changing roughly every 5 days. Two cases, 'gas-phase' and 'sulphate', are shown. For the heterogeneous reactions (4) and (5) on sulphate-layer aerosols, I adopt reaction probabilities of 0.01 and 0.1, respectively, with surface area $\sim 2.5 \times 10^{-8}$ cm^2 cm^{-3}. The model was re-initialized on 29 July with conditions ($O_3 = 2.5 \times 10^{-6}$, $H_2O = 2 \times 10^{-6}$, $HNO_3 = 2 \times 10^{-9}$, $NO_x = ClONO_2 = 0$, $HCl = 1.2 \times 10^{-9}$, $ClO_x = 0.7 \times 10^{-9}$, $HOCl = 0.6 \times 10^{-9}$ (denoted 'winter HOCl') and with alternative conditions ($HOCl = 0$, $ClO_x = 1.3 \times 10^{-9}$) with results shown in Table 1. The 'standard' PSC chemistry reactions (2) and (3) were integrated through the spring at their effective rate limits, $k = 1 \times 10^{-11}$ cm^3 s^{-1}, yielding maximum conversion to ClO_x (see text and Table 1). The 'new' PSC chemistry includes in addition reaction (1). The photochemical model is documented in refs 43, 44. The calculations use climatological mean temperatures and ozone profiles for the photolysis rates. I assume an atmosphere of 1,000 mbar, a surface albedo of 0.30, fully spherical solar extinction, and Rayleigh-phase scattering in a plane-parallel atmosphere.
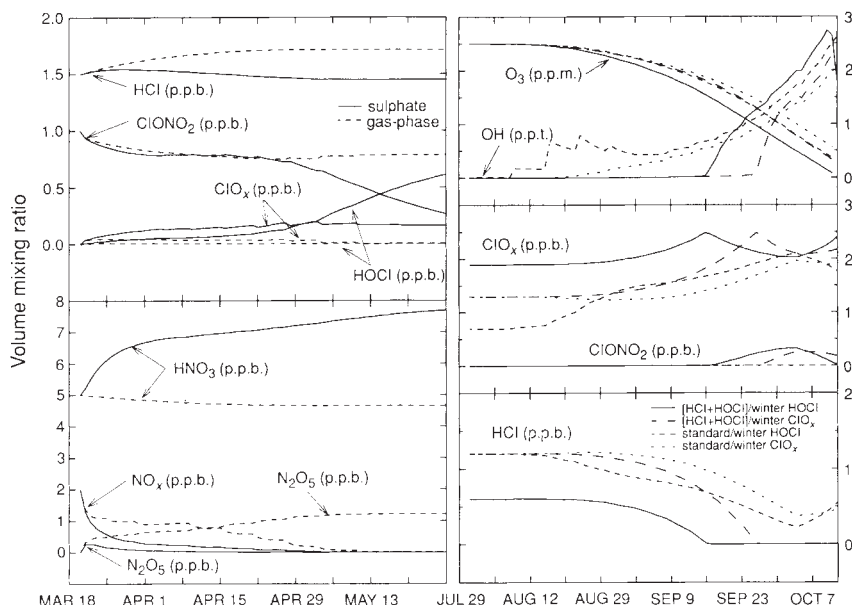
TABLE 1 Chemical rate limits

Reaction (1)*	
$O(^1D) + H_2O$ (×2)	$44\ cm^{-3}\ s^{-1}$
$O(^1D) + H_2$ (×2)	5
CH_4 oxidation cycle	505
HNO_3 + photon	171
$HNO_3 + OH$ (×−1)	−8
net production of HO_x	$725\ cm^{-3}\ s^{-1}$
$HO_2 + ClO \rightarrow HOCl + O_2$	720
$HOCl + HCl(PSC)$	720
24-h average OH	$5.8 \times 10^3\ cm^{-3}$
24-h average HO_2	$3.2 \times 10^4\ cm^{-3}$
Reaction (2)†	
HNO_3 + photon	$171\ cm^{-3}\ s^{-1}$
$HNO_3 + OH$	248
net production of NO_x	$419\ cm^{-3}\ s^{-1}$
$ClONO_2 + HCl(PSC)$	418
24-h average OH	$1.9 \times 10^5\ cm^{-3}$
24-h average HO_2	$4.0 \times 10^5\ cm^{-3}$

Latitude 75° S at 20 km with solar declination of +6° (10 September).
* In the saturation limit $k_{HCl+HOCl} > 1 \times 10^{-12}\ cm^3\ s^{-1}$.
† In the saturation limit $k_{HCl+ClONO_2} > 5 \times 10^{-13}\ cm^3\ s^{-1}$.

considered: a 'standard' model with reactions (2) and (3), and a 'new' model that also includes reaction (1). The initial conditions, taken from the March–May calculations, include a large abundance of HOCl ('winter HOCl'), which in the 'new' model rapidly oxidizes a large fraction of the HCl. For a better comparison of the 'standard' and 'new' PSC chemistries, I also include an initialization without HOCl, in which the HOCl generated from reaction (4) during polar night is arbitrarily converted to ClO.

Limits to the effectiveness of PSC chemistry are found through a sensitivity study that identifies the key gas-phase chemical rates responsible for liberation of ClO_x. I treat the PSC reactions (1) to (3) as effective two-body rates with coefficients k_1, k_2 and k_3, ranging from 0 to $1 \times 10^{-11}\ cm^3\ s^{-1}$. In September, the effect of reaction (2) alone is negligible for $k_2 < 1 \times 10^{-15}\ cm^3\ s^{-1}$ and saturates for $k_2 > 5 \times 10^{-13}\ cm^3\ s^{-1}$. This range of two-body rates corresponds to reaction probabilities for $ClONO_2$ of ~0.001–0.5 for typical PSC surface areas[40] of $2 \times 10^{-7}\ cm^2\ cm^{-3}$ and 1 p.p.b. of HCl. In the upper limit, oxidation of HCl is maximal and is limited by the production of $ClONO_2$, which is in turn limited by release of NO_x from destruction of HNO_3 by photons or OH reactions. Critical rates in this limit are summarized in Table 1.

Reaction (1) has considerable impact on the HO_x chemistry, reducing OH and HO_2 concentrations by 40% even for k_1 as low as $1 \times 10^{-16}\ cm^3\ s^{-1}$. Its effect saturates for $k_1 > 1 \times 10^{-12}\ cm^3\ s^{-1}$, and the rate of reaction (1) is limited by the production of $HO_x(OH + HO_2 + 2 \times H_2O_2)$ because HOCl is produced by reaction of HO_2 with ClO and reaction (1) is the dominant sink for HO_x. Most HO_x is produced by primary reactions of $O(^1D)$ with H_2O, H_2 and CH_4, followed by amplification through the CH_4 oxidation cycle (for example, one OH begets two or more HO_2 as CH_4 is oxidized to CO); but an important fraction can come from HNO_3 photolysis. The rate-limiting reactions are shown in Table 1.

In the calculations shown in Fig. 1, the upper limits for PSC reaction rates are used, and thus the increase in ClO_x and the corresponding decrease in O_3 are the largest possible, being limited by the amount of sunlight. The densities of N_2O_5 and NO_x remain low throughout this period because of the effectiveness of reaction (2): any odd-nitrogen not tied up as HNO_3 is in the form of $ClONO_2$. Therefore reaction (3), even at PSC

rates, is unimportant. Similarly, reactions (4) and (5), continued as sulphate-layer chemistry, are not important.

With the 'new' PSC chemistry (reaction 1), concentrations of ClO_x (excepting the initial reaction of winter HOCl) begin to increase by 26 August and continue for 3–4 weeks until the HCl supply is exhausted. Both OH and $ClONO_2$ concentrations are suppressed until the HCl disappears (see below). Ozone losses become constant, ~50–60 p.p.b. per day, independent of the O_3 abundance. This unusual property of Cl_2O_2-catalysed ozone loss occurs when ClO_x is the dominant chlorine species and thus Cl_2O_2 densities are independent of O_3 densities; it allows for the more rapid linear loss, rather than exponential decay, to less than 0.2 p.p.m. O_3 as observed[7]. With the 'standard' PSC chemistry (reaction 2), increases in ClO_x (again excepting the early photolysis of winter HOCl) do not begin until 9 September and never reach values as high as with reaction (1). The rapid loss of O_3 is delayed by five days, and ClO_x concentrations begin to decline as HCl recovers in October.

Concentrations of OH and HO_2 are an important diagnostic of the proposed mechanism, because OH is suppressed by reaction (1). In contrast, reaction (2) has little effect on HO_x: noontime OH concentrations climb to $1 \times 10^6\ cm^{-3}$ in the first week of September, and without reaction (1) the winter HOCl provides a pulse of OH in early August. Concentrations of HOCl or $ClONO_2$ are poor tests of the proposed mechanisms: in the saturation limit, the rate of HCl oxidation is independent of the PSC activity, but the densities of HOCl and $ClONO_2$ are inversely proportional to PSC surface area. The low column-abundances of HOCl observed in late September[41] are consistent with all of these calculations, in which noontime HOCl densities range from 1 to $3 \times 10^8\ cm^{-3}$.

The timing of the rapid ClO_x increase in these calculations is appropriate to the mean insolation at 75° S. At a latitude of 70° S, the increase in sunlight would occur about 12 days earlier. During this chemical evolution, one expects that the air parcels remain neither isolated nor at one latitude. Lagrangian trajectories show latitudinal excursions[42], and wind shear plus molecular diffusion will lead to mixing of parcels[43]. Neither of these processes would affect the basic results shown here, but they might alter the mean insolation, or effective latitude of the air parcel.

The oxidation of HCl by HOCl (reaction 1) always exceeds that by $ClONO_2$ (reaction 2), often by more than a factor of 2. Furthermore, the HOCl pathway becomes effective at 75° S by the end of August, well before the $ClONO_2$ mechanism. The upper limit of ClO_x growth by reaction (2) is almost linearly proportional to the gas-phase abundance of HNO_3; but if HNO_3 is tied up as solid $HNO_3 \cdot 3H_2O$ (type I PSCs) and cannot be photodissociated, then reaction (2) becomes ineffective. A simple cycling of HNO_3 between PSCs and gas phase due to parcel trajectories[44] can circumvent this impasse, but would further lengthen the time needed to oxidize HCl.

Heterogeneous reactions involving HOCl are therefore important in creating high concentrations of ClO_x, and hence O_3 losses, during early spring in the polar stratosphere. The oxidation of HCl into forms of ClO_x requires that PSCs be prevalent, but the growth in ClO is limited by the photochemical production of the oxidant (HOCl or $ClONO_2$) and cannot be accelerated beyond this limit by known microphysical processes on stratospheric clouds. □

1. Stumm, W. & Morgan, J. J. Aquatic Chemistry (Wiley, New York, 1981).
2. Molina, M. J., Ishiwata, T. & Molina, L. T. J. phys. Chem. 84, 821–825 (1980).
3. Hanson, D. R. & Ravishankara, A. R. J. phys. Chem. (submitted).
4. Abbatt, J. P. D. & Molina, M. J. Geophys. Res. Lett. (submitted).
5. Farman, J. C., Gardiner, B. G. & Shanklin, J. D. Nature 315, 207–210 (1985).
6. Stolarski, R. S. et al. Nature 322, 808–811 (1986).
7. Hofmann, D. J. et al. Nature 326, 59–62 (1987).
8. Rowland, F. S., Sato, H., Khwaja, H. & Elliott, S. M. J. phys. Chem. 90, 1985–1988 (1986).
9. Molina, M. J., Tso, T. L., Molina, L. T. & Fang, F. C. Y. Science 238, 1253–1258 (1987).
10. Tolbert, M. A., Rossi, M. J., Malhotra, R. & Golden, D. M. Science 238, 1258–1261 (1987).

11. Solomon, S., Garcia, R. R., Rowland, F. S. & Wuebbles. D. J. *Nature* **321**, 755–758 (1986).
12. McElroy, M. B., Salawitch, R. J., Wofsy, S. C. & Logan, J. A. *Nature* **321**, 759–762 (1986).
13. Molina, L. T. & Molina, M. J. *J. phys. Chem.* **91**, 433–436 (1986).
14. Hayman, G. D., Davies, J. M. & Cox, R. A. *Geophys. Res. Lett.* **13**, 1347–1350 (1988).
15. Sander, S. P., Friedl, R. R. & Yng, Y. L. *Science* **245**, 1095–1098 (1989).
16. Solomon, S., Mount, G. H., Saunders, R. W. & Schmeltekopf, A. L. *J. geophys. Res.* **92**, 8329–8388 (1987).
17. de Zafra, R. L. *et al. Nature* **329**, 408–411 (1987).
18. Brune, W. H., Anderson, J. G. & Chan, K. R. *J. geophys. Res.* **94**, 16649–16663 (1989).
19. Anderson, J. G., Brune, W. H. & Proffitt, M. H. *J. geophys. Res.* **94**, 11465–11479 (1989).
20. Anderson, J. G., Brune, W. H. & Toohey, D. W. *Science* **251**, 39–46 (1991).
21. Brune, W. H. *et al. Science* **252**, 1260–1266 (1991).
22. Rodriguez, J. M. *et al. J. geophys. Res.* **94**, 16683–16703 (1989).
23. Austin, J. *et al. J. geophys. Res.* **94**, 16717–16735 (1989).
24. Mozurkewich, M. & Calvert, J. G. *J. geophys. Res.* **93**, 15889–15896 (1988).
25. Tolbert, M. A., Rossi, M. J. & Golden, D. M. *Geophys. Res. Lett.* **15**, 847–850 (1988).
26. Van Doren, J. M. *et al. J. phys. Chem.* **95**, 1684–1689 (1991).
27. Hanson, D. R. & Ravishankara, A. R. *J. geophys. Res.* **96**, 17307–17314 (1991).
28. Prather, M. J. & Rodriguez, J. M. *Geophys. Res. Lett.* **15**, 1–4 (1988).
29. Leu, M. T. *Geophys. Res. Lett.* **15**, 17–20 (1988).
30. Leu, M. T. *Geophys. Res. Lett.* **15**, 851–854 (1988).
31. Quinlan, M. A., Reihs, C. M., Golden, D. M. & Tolbert, M. A. *J. phys. Chem.* **94**, 3255–3260 (1990).
32. Van Doren, J. M. *et al. J. phys. Chem.* **94**, 3265–3269 (1990).
33. Hanson, D. R. & Ravishankara, A. R. *J. geophys. Res.* **96**, 5081–5090 (1991).
34. Hofmann, D. J. & Solomon, S. *J. geophys. Res.* **94**, 5029–5041 (1989).
35. Brasseur, G. P., Granier, C. & Walters, S. *Nature* **348**, 626–628 (1990).
36. Mather, J. H. & Brune, W. H. *Geophys. Res. Lett.* **17**, 1283–1286 (1990).
37. Rodriguez, J. M., Ko, M. K. W. & Sze, N. D. *Nature* **352**, 134–137 (1991).
38. Keys, J. G. *et al. Geophys. Res. Lett.* **13**, 1260–1263 (1986).
39. Fahey, D. W. *et al. Nature* **344**, 321–324 (1990).
40. Toon, O. B., Browell, E. V., Kinne, S. & Jordan, J. *Geophys. Res. Lett.* **17**, 393–396 (1990).
41. Toon, G. C. & Farmer, C. B. *Geophys. Res. Lett.* **16**, 1375–1377 (1989).
42. Jones, R. L. *et al. J. geophys. Res.* **94**, 11529–11558 (1989).
43. Prather, M. J. & Jaffe, A. H. *J. geophys. Res.* **95**, 3473–3492 (1990).
44. deMore. W. B. *et al. JPL 90-1* NASA Jet Propulsion Laboratory. 1990).

Link between iron and sulphur cycles suggested by detection of Fe(II) in remote marine aerosols

Guoshun Zhuang*‡, **Zhen Yi**†, **Robert A. Duce***‡ **& Phyllis R. Brown**†

* Center for Atmospheric Chemistry Studies, Graduate School of Oceanography, University of Rhode Island, Narragansett, Rhode Island 02882, USA
† Department of Chemistry, University of Rhode Island, Kingston, Rhode Island 02881, USA

IRON is essential to the growth of organisms, and iron derived from the atmosphere may be the limiting nutrient for primary productivity in some oceanic regions[1–6]. Aeolian mineral dust is the chief source of marine iron in many areas[1–3,5,7], but there is little information on the chemical form of the iron in this dust. Here we report that Fe(II) contributed $56 \pm 32\%$ of the total iron in marine aerosol samples collected over the central North Pacific and $49 \pm 15\%$ at Barbados. We suggest that the key reaction that produces Fe(II), and hence increases the solubility of marine aerosol iron in sea water, is $[Fe(III)(OH)(H_2O)_5]^{2+} + H_2O \xrightarrow{h\nu} [Fe(II)(H_2O)_6]^{2+} + OH\cdot$ (refs 8–10). The presence of Fe(II) in remote marine aerosols suggests that the OH radical has been produced in these heterogeneous reactions. From consideration of both the marine biological production of dimethylsulphide and the subsequent oxidation of reduced forms of sulphur in the atmosphere, we propose that the iron and sulphur cycles in both the atmosphere and the ocean may be closely coupled.

We collected atmospheric aerosol samples continuously for one-week periods during 1986 using high-volume air-sampling systems and Whatman 41 filters (20×25 cm) at four North

Pacific island stations (Midway, Oahu, Enewetak and Fanning). We also collected aerosol samples at Barbados in the North Atlantic in September and October 1988 and April 1990. Urban aerosol samples were collected during November 1989 in the city of Xian ($34°$ N, $109°$ E) in central China near the loess plateau region. Samples of loess were collected at Luochuan ($35.5°$ N, $109°$ E), China, in the loess plateau region, an important source area for the mineral aerosol particles found over the North Pacific. All samples were stored in the dark and frozen from the time of collection until analysis.

Iron(II) concentrations in aerosols and Chinese loess were determined by high-performance liquid chromatography (HPLC)[11]. A considerable proportion of the iron in the aerosols was in the form of Fe(II) (see Fig. 1). Concentrations of Fe(II) over the North Pacific ranged from 11% to nearly 100% of the total iron, $T(Fe)$. The volume-weighted mean Fe(II) concentration was $56 \pm 32\%$ of $T(Fe)$ at the North Pacific sites and $49 \pm 15\%$ at Barbados. The $T(Fe)$ at Barbados was ~ 0.6–$5 \mu g \, m^{-3}$, whereas $T(Fe)$ at the North Pacific sites was ~ 0.010–$0.15 \mu g \, m^{-3}$. Although the percentage of Fe(II) in some of the Barbados samples was less than 10%, the Fe(II) concentrations were in the range of ~ 28–$150 \, ng \, m^{-3}$, similar to the Fe(II) concentration range of 5–$135 \, ng \, m^{-3}$ in the North Pacific samples.

The urban aerosol samples from Xian contained 4–11% Fe(II), with a volume-weighted average of $5 \pm 3\%$. (In urban fog samples from Zurich, 20–90% of the total iron was present as Fe(II)[12].) Samples of Chinese loess contained only $0.4 \pm 0.3\%$ Fe(II). During atmospheric transport over $\sim 10,000$ km from central Asia to the central North Pacific, the Fe(II) fraction of $T(Fe)$ increased from less than 1% in the Chinese loess to more than 50% in the marine aerosols (see Table 1). The solubility of iron in these same marine aerosols in acidified water (pH = 2.0–5.6) was 5–17 times higher than the iron in Chinese loess[11].

Is the Fe(II) in remote marine aerosols simply small-particle Fe(II) produced in the source area, which becomes increasingly important as the large particles are lost during long-range transport, or is it produced by transformation processes during the long-range transport? Lead can be used as a reference to compare with Fe(II), as lead over the North Pacific is derived largely from anthropogenic sources in Asia and is found primarily on small, submicrometre aerosol particles[13]. Lead in a typical urban area such as Beijing[14] ranged from 52 to 257 ng m^{-3}. Observed lead concentrations over the central North Pacific ranged from a mean of 2 ng m^{-3} at Oahu[15] to ~ 0.33–1.1 ng m^{-3} between $20°$ and $50°$ N (ref. 16) This indicates that lead, representative of small particles, decreased by a factor of more than 100 during
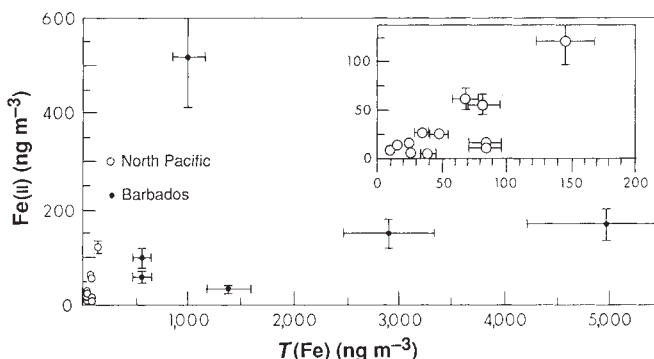

FIG. 1 Fe(II) concentration as a function of total iron concentration, $T(Fe)$, in remote marine aerosols from islands in the North Pacific and from Barbados in the North Atlantic. The peak of the Fe(II) complex with ferrozine (FZ), $[Fe(II)(FZ)_3]^{2+}$, in the HPLC measurement was identified by retention time, by the addition of known quantities of standard and by comparing the peak ratios at various wavelengths.

537